RSC Advances

PAPER

View Article Online
View Journal | View Issue

Cite this: *RSC Adv.*, 2020, **10**, 32193

Unusual features of nitrogen substitutions in silicene

Hai Duong Pham,*[a] Godfrey Gumbs,[b] Wu-Pei Su,[c] Ngoc Thanh Thuy Tran[d] and Ming-Fa Lin *[a]

The quasiparticle properties resulting from charge and spin are clearly identified in nitrogen-substituted silicenes, for which a theoretical framework is successfully developed from first-principles calculations. Such systems create extremely non-uniform chemical and physical environments through the distribution of the guest atoms. They present unusual geometric, electronic, and magnetic properties, which can be identified from the optimal honeycomb lattices, the atom- and spin-dominated energy spectra, the spatial charge density distributions, and the atom-, orbital- and spin-projected van Hove singularities [the net magnetic moments]. The complicated relations between the highly hybridized sp^2-N–Si bonds and the ferromagnetic/non-magnetic configurations are responsible for the p-type or semiconducting behavior, the significant modifications to the Dirac cone structures, the difficulty in identifying the π and σ bands, and the vanishing or finite magnetic moments. The theoretical predictions could be verified by high-resolution experimental measurements.

Received 19th May 2020
Accepted 9th August 2020

DOI: 10.1039/d0ra04470a

rsc.li/rsc-advances

1 Introduction

Both group-IV and group-V systems have been successfully synthesized on distinct substrates since the first discovery of monolayer graphene by mechanical exfoliation of a graphite surface in 2004,[1] such as layered silicene on Ag(111)/Ir(111)/ZrB_2 surfaces,[2–4] and germanene on Pt(111)/Au(111)/Al(111) surfaces.[5–7] Apparently, they are mainstream 2D materials that exhibit diverse physical/chemical/material properties,[8,9] clearly illustrating their critical role in basic and applied sciences. It is well known that C, Si, Ge, Sn, and Pb atoms present four half-occupied orbitals in condensed-matter systems, respectively covering [2s, $2p_x$, $2p_y$, $2p_z$], [3s, $3p_x$, $3p_y$, $3p_z$], [4s, $4p_x$, $4p_y$, $4p_z$], [5s, $5p_x$, $5p_y$, $5p_z$], and [6s, $6p_x$, $6p_y$, $6p_z$]. In general, they can generate π, σ and sp^3 chemical bonding. These atomic configurations are quite different from those of the isolated atoms; therefore, the material surfaces are able to provide very active chemical environments. Diverse properties are easily achieved by modulating various critical factors including lattice symmetries,[10,11] planar/buckled/curved geometries,[12,13] stacking configurations [simple/greatly enlarged unit cells[14]], chemical adatom adsorption,[15] guest atom substitutions,[16] defects/vacancies,[17] quantum confinement and edge structures,[18] heterojunctions,[19] gate voltages,[20] magnetic fields,[21] and mechanical strain.[22] In this paper, a theoretical framework built from first-principles calculations is developed to comprehend the highly diverse essential properties of nitrogen-substituted silicene systems, especially the charge-[23] and spin-created quasiparticle behavior.[24]

Chemical modifications, which include substitution[16] and adsorption,[25] are very efficient in creating totally different condensed-matter systems or inducing significant modifications of the pristine lattice through strong host–guest multi-orbital hybridizations and significant atom-induced spin distributions. Such methods are suitable for surface manipulations of 2D emergent materials. Specifically, many graphene-related materials have recently been produced in laboratories, *e.g.*, halogenated and hydrogenated graphene systems[26,27] and graphene oxides.[28,29] There are also some experimental and theoretical studies on silicene-based compounds. For example, rare earth layers, with thicknesses ranging from a thin film down to a monolayer, are shown to present a dramatic anti-ferromagnetism to ferromagnetism transition.[30] That is, a class of robust 2D magnets is generated in the synthesis. On the theoretical side, first-principles calculations are utilized to explore the substitution- and adsorption-enriched essential properties, *e.g.*, the diverse phenomena in N-, B-, C-, Al-, P-,[31] transition-metal-,[23] CO_2-/H_2S-/SO_2-containing silicene systems.[32] N-substituted silicene, in some specific configurations, is predicted to be a ferromagnetic metal.[31] However, the sensitive concentration and configuration dependencies and the critical physical/chemical/material mechanisms are not clear. Systematic investigations of these are conducted in this work.

[a]*Department of Physics, National Cheng Kung University, 701 Tainan, Taiwan. E-mail: phamduong477@gmail.com; mflin@mail.ncku.edu.tw*

[b]*Department of Physics and Astronomy, Hunter College of the City University of New York, 695 Park Avenue, New York, New York 10065, USA*

[c]*Department of Physics, University of Houston, Houston, 77204 Texas, USA*

[d]*Hierarchical Green-Energy Materials (Hi-GEM) Research Center, National Cheng Kung University, Tainan 70101, Taiwan*

Our study covers the extremely non-uniform physical and chemical environments, the absence/existence of Si–Si, Si–N and N–N bonds, the bond-length modulations, the fully destroyed/modified Dirac cone structures, the semiconducting or semi-metallic/metallic properties, well-defined or irregular doping cases, p- or n-type doping, identification of the π- and σ-electronic properties [*e.g.*, their band widths] and the ferromagnetic/non-magnetic/anti-ferromagnetic configurations. The theoretical predictions of the nitrogen-substitution-enriched geometries, band structures, van Hove singularities and net magnetic moments could be verified through high-resolution scanning tunneling microscopy/transmission electron microscopy [STM/TEM],[33] angle-resolved photoemission spectroscopy [ARPES],[34] scanning tunneling spectroscopy [STS],[35] and superconductor quantum interference device [SQUID][36] measurements.

2 Computational details

The unusual features of nitrogen substitutions in silicene are investigated in detail by using the VASP code.[37,38] The exchange and correlation energies due to many-particle electron–electron interactions are calculated with the use of the Perdew–Burke–Ernzerhof (PBE) functional under the generalized gradient approximation.[39] Furthermore, the electron–ion interactions can be characterized by the projector augmented wave (PAW) pseudopotentials.[40] A space of 15 Å width is inserted between the silicene planes to avoid their interaction. In general, a plane-wave basis set with a maximum kinetic energy cutoff of 500 eV is chosen to expand the wave function. The first Brillouin zone is sampled by $9 \times 9 \times 1$ and $100 \times 100 \times 1$ *k*-point meshes within the Monkhorst–Pack scheme for further calculations of the electronic and magnetic properties. The energy convergence is set to be 10^{-5} eV between two consecutive steps and the maximum Hellmann–Feynman force acting on each atom is less than 0.01 eV $Å^{-1}$ during the ionic relaxations.

3 Results and discussions

3.1 Geometric structures

The nitrogen-substituted silicene systems exhibit very unique geometries [Fig. 1 and Table 1]. To achieve the optimal geometric structures, the spin-dependent many- and single-particle interactions, which respectively correspond to the on-site Coulomb and spin-orbital interactions,[41] need to be included in the first-principles calculations. Extremely non-uniform bond lengths are observed in enlarged unit cells except for the pristine and [1 : 1] cases [Fig. 1(a)]. The N–N bonds, with length ∼1.418 Å [Table 1], are stable in the [2 : 4]-*ortho* case [Fig. 1(d)]. However, the opposite is true for the [2 : 6]- and [2 : 16]-*ortho* cases [Fig. 1(f) and (i)], in which the nitrogen atoms are too far apart to form a bond. Furthermore, buckled geometries are observed for various concentrations and configurations [Fig. 1(a)–(l)]. Roughly speaking, the maximum height difference between the A and B sublattices is bigger than that in the absence of nitrogen substitution. These features might be closely related to the multi-orbital hybridizations of

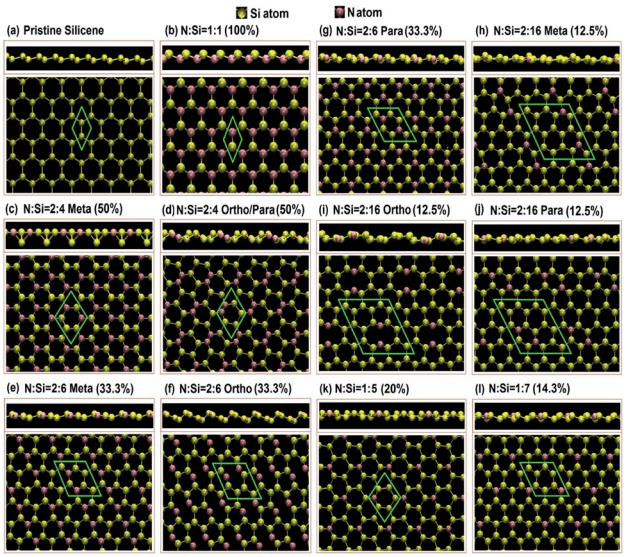

Fig. 1 The top and side views of the optimal geometric structures for nitrogen-substituted silicene systems in (a) pristine, (b) full, (c) 50%-*meta*, (d) 50%-*ortho*/*para*, (e) 33.3%-*meta*, (f) 33.3%-*ortho*, (g) 33.3%-*para*, (h) 12.5%-*meta*, (i) 12.5%-*ortho*, (j) 12.5%-*para*, (k) 20%-single and (l) 14.3%-single substitution cases.

the ill-defined π and σ chemical bonds [discussed later in the spatial charge density section]. The highly asymmetric chemical environments, which are characterized by the observable fluctuation ranges of N–Si/Si–Si bond lengths and buckled structures, are expected to create complicated charge distributions and thus diversify the other essential properties.[42]

3.2 Electronic band structures

The nitrogen atoms, with five valence electrons in the 2s, $2p_x$, $2p_y$, and $2p_z$ orbitals, can create unusual substitution effects on the silicene-based electronic states [Fig. 2(a)–(l)], mainly owing to the complicated multi-orbital hybridizations in the N–Si/Si–Si/N–N bonds, the enhanced buckling of the two sublattices, and the ferromagnetic spin configuration. The electronic structures are very sensitive to changes in the N concentration. For the [1 : 1] case [Fig. 1(b) and 2(b)], the uniform 2D nitrogen-silicene compound is an indirect-gap semiconductor with a unique ferromagnetic spin configuration. The lowest unoccupied conduction state is located at the Γ point, while the highest occupied valence state is located in between the Γ and K points. There is an indirect band gap E_g^i of ∼0.21 eV. The occupied and unoccupied electronic bands are highly asymmetric about the Fermi level, clearly illustrating the complex hopping integrals and site energies as a result of the strong interactions of the atom-dependent orbitals. Obviously, a modified Dirac cone structure near E_F is totally absent. This indicates that the original π bonding in pristine silicene has undergone a dramatic transformation [discussed later for the charge distribution in Fig. 3(b)]. It is almost impossible to trace the initial, intermediate, and final π-bands along the high-symmetry paths. A full investigation of the π-band widths becomes meaningless. Similar phenomena could be found in

Table 1 The optimal geometric structures of nitrogen-substituted silicene systems at various concentrations and configurations with the N–N, N–Si, and Si–Si bond lengths, the band gaps, and the ground state energies per unit cell, together with the height differences between the A and B sublattices

Number of atoms/unit cell	Percentage	Ratio of N/Si	N–N bond length (Å)	N–Si bond length (Å)	Nearest Si–Si distance (Å)	Second nearest Si–Si distance (Å)	Magnetic moment (μ_B)	E_g^d (eV)/metal	Optimized E_0 (eV)	Δ (Å)
2	✗	Pristine	✗	✗	2.250	✗		0.001	−9.307	0.48
	100%	[1 : 1]	✗	1.783	✗	✗	0.25	0.268	−13.783	0.57
6	50%	[2 : 4]-*meta*	✗	1.800	2.367	✗	1.06	Semi-metal	−36.794	0.9
	50%	[2 : 4]-*ortho*/*para*	1.418	1.783	2.307–2.365	✗	0	Semi-metal	−34.874	0.65
	20%	[1 : 5]	✗	1.781	2.306	✗	0.51	0.087	−32.540	0.7
8	33.3%	[2 : 6]-*meta*	✗	1.765–1.926	2.241	2.425	0	Semi-metal	−44.510	0.45
	33.3%	[2 : 6]-*ortho*	3.103	1.654	2.349	2.300	0	Semi-metal	−45.017	0.88
	33.3%	[2 : 6]-*para*	✗	1.809	2.373	✗	0	Semi-metal	−46.041	0.41
	14.3%	[1 : 7]	✗	1.819	2.273	2.201	0.11	Semi-metal	−41.076	0.63
18	12.5%	[2 : 16]-*meta*	✗	1.738–2.301	2.290–2.436	2.247–2.448	0	0.31	−91.682	0.38–0.68
	12.5%	[2 : 16]-*ortho*	3.491	1.672	2.324–2.426	2.262–2.325	0	Semi-metal	−92.179	0.44–0.78
	12.5%	[2 : 16]-*para*	✗	1.836	2.266–2.292	2.289–2.426	0	Semi-metal	−92.883	0.2–0.41
	5.8%	[1 : 17]	✗	1.830	2.315	2.264–2.329	0	Semi-metal	−88.810	0.35–0.65

the σ-bands, clearly illustrating the absence of well-defined π and σ chemical bonding.

The electronic energy spectrum shows non-monotonic wave-vector dependence, in which the band-edge states might appear in between two high-symmetry points. This result is reflected in the rich van Hove singularities of the density of states and optical excitation spectra.[43] Most importantly, the spin degeneracy is destroyed by the spin-induced many-body effects [the on-site Coulomb interactions in the Hubbard-like model].[44] The ferromagnetic spin distributions are associated with the host and guest atoms [the spin density distributions are shown in Fig. 4(a)–(d)]. The spin-up and spin-down energy sub-bands have observable spacings of $E_s \sim 0.1$–2.0 eV, which can be examined through spin-polarized ARPES and STS measurements.

In general, the spin-split energy sub-bands which are more than 1.50 eV apart are either both occupied or unoccupied states. As a result, such pairs do not contribute to the net magnetic moments. On the other hand, the valence and conduction bands closest to the Fermi level respectively arise from the spin-up and spin-down configurations [the red and black curves]. The former can create a ferromagnetic configuration in the buckled honeycomb lattice [Table 1] and thus a large magnetic moment per unit cell. Very interestingly, each sub-band is dominated by both silicon and nitrogen atoms, as seen from the size of the blue circles and green triangles representing the silicon and nitrogen contributions, respectively. It would be very difficult to distinguish between the N- and Si-dominated energy sub-bands by experimental measurements.[46] The magnetic properties are determined by both the host and guest atoms. This would make it very difficult to adopt a tight-binding model, *i.e.*, the multi-orbital-dependent hopping integrals, ionization energies, and on-site Coulomb interactions would become very complex.[47]

3.3 Spatial charge density and spin density distributions

The ferromagnetic bands deserve a closer examination. They exist in certain cases with sufficiently high nitrogen concentrations, such as [2 : 4]-*meta*, [1 : 5] and [1 : 7] [Fig. 2(c), (k) and (l)]. The [2 : 4]-*meta* and [1 : 7]/[1 : 5] nitrogen substitution cases exhibit metallic [or semi-metallic] behavior. Their ferromagnetic configurations are, respectively, dominated by two and one pairs of spin-split valence and conduction bands near the Fermi level. Whether these energy sub-bands cross E_F will determine the existence of free carriers and their densities. Furthermore, they are closely related to the relative contributions of the host and guest atoms. The silicon and nitrogen atoms might have distinct weights and even opposite signs in the spin density distributions [discussed later in Fig. 4(a)–(d)]. Only nitrogen-substituted silicene systems are capable of displaying ferromagnetic spin configurations, as opposed to the carbon- and boron-containing ones.[48]

Whether nitrogen-substituted silicenes present spin-split energy sub-bands, as well as finite-gap or gapless behavior, strongly depends on the concentration and arrangement of guest atoms. Non-magnetic band structures also exist in high-

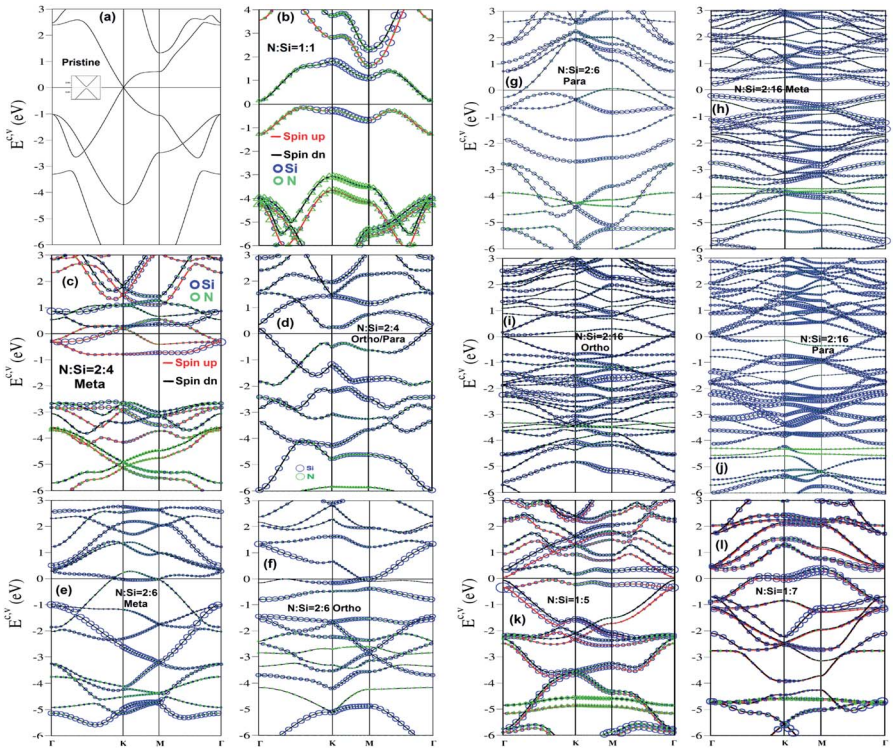

Fig. 2 Electronic band structures of the nitrogen-substituted silicene systems, showing the dominance of N and Si atoms [the green triangles and blue circles, respectively], for the substitution cases: (a) no substitution, (b) [1 : 1], (c) [2 : 4]-*meta*, (d) [2 : 4]-*ortho*/*para*, (e) [2 : 6]-*meta*, (f) [2 : 6]-*ortho*, (g) [2 : 6]-*para*, (h) [2 : 16]-*meta*, (i) [2 : 16]-*ortho*, (j) [2 : 16]-*para*, (k) [1 : 5]-single, (l) [1 : 7]-single.

concentration cases, *e.g.*, the [2 : 4]-*ortho*/*para*, [2 : 6]-*meta*, [2 : 6]-*ortho* and [2 : 6]-*para* cases, as clearly indicated in Fig. 2(d)–(g). This result suggests that the spin-dependent on-site Coulomb interactions are strongly suppressed by the complicated multi-orbital hybridizations in Si–Si, N–Si, and N–N chemical bonds. Most importantly, the semiconducting or semi-metallic/metallic behavior, is mainly determined by the low-lying energy sub-bands with complicated dispersion. For example, the three 33.3% cases exhibit partially flat sub-bands across the Fermi level, thus they are expected to have a large density of states at E_F [discussed later in Fig. 5(e)–(g)]. It should also be noted that it is almost impossible to recognize n- or p-type doping in the nitrogen-substituted silicene systems from the complicated low-lying sub-bands. That is to say, the valence electron number cannot be utilized to characterize the substitution-induced free carriers. Ferromagnetic configurations are absent at sufficiently low concentrations, as illustrated by the [2 : 16]-*meta*, [2 : 16]-*ortho*, [2 : 16]-*para*, and [1 : 17] configurations in Fig. 2(h), (i), (j) and (l), respectively. Very interestingly, the modified linear valence and conduction sub-bands [the modified Dirac cone structures] are located near the Γ point. They are related to the van Hove singularities close to E_F [Fig. 5(h)–(j) and (l)]. They should be dominated by pure and hybridized π bonding. However, the band structures are too complex to characterize by π- and σ-band widths. No well-behaved chemical bonding can be deduced in the nitrogen-substituted silicenes.

Apparently, the calculated band structures are very complicated for the nitrogen-substituted silicene systems. It would be difficult to reproduce them from a tight-binding model with complex multi-orbital hopping integrals and site energies,[41] even with the Hubbard-like spin-induced on-site Coulomb interactions.[44] That is, phenomenological models might not be able to provide a critical mechanism and a concise picture of the essential properties. For example, the generalized tight-binding model,[45] which includes magnetic-field effects, cannot be utilized to explore the unique magnetic quantization phenomena. As a result, first-principles calculations are the only way to fully understand the diverse phenomena.

Although the calculated electronic energy spectra are very complex, they can be verified by careful examination by ARPES and SP-ARPES. The former is very successful in identifying the electronic structures of layered materials, *e.g.*, the dimension-diversified energy bands in bulk graphites,[49] graphenes,[50] graphene nanoribbons,[51] and substrate-enriched few-layer group-IV systems.[52] The latter has confirmed the spin-resolved occupied energy sub-bands of topological insulators,[53] ferromagnetic materials,[54] and superconductors.[55] Experimental examinations of the nitrogen-substituted silicene systems can focus on the oscillatory energy dispersions near the Fermi level, the non-magnetic or ferromagnetic electronic states, the gapless or finite-gap band properties, and the modified/absent Dirac cone band structure at sufficiently low/high guest-atom concentrations. The measured results could provide important information closely related to the complex relations among

the π, sp^2, and sp^3 bonding, and the strong competition/cooperation between the multi-orbital hybridizations and the spin configurations.

The nitrogen-substituted silicene systems exhibit unique charge density distributions, compared with the pristine one. The charge density is highly asymmetric about the center of the N–Si bond in the [*x*, *y*]-, [*x*, *z*]- and [*y*, *z*]-plane projections. Most of the charge is accumulated around the nitrogen atoms, which affects the formation of the π bonds. The N–Si bonds are estimated to have significant and complicated [2s, $2p_x$, $2p_y$, $2p_z$]–[3s, $3p_x$, $3p_y$, $3p_z$] sp^3-orbital hybridizations. That is to say, it is very difficult to characterize the σ- and π-electronic bonding. There are also Si–Si and N–N bonds when the nitrogen concentration decreases [Fig. 3(c)–(h)]. Apparently, the charge distributions between two identical atoms are seriously distorted compared with the pristine case. For example, the rectangular σ-distribution, which is present in the pristine silicene [the [*x*, *y*]-plane projection in Fig. 3(a)], dramatically changes into a triangular one upon nitrogen substitution. Serious distortions are also revealed in the π-bonding. The pure orbital hybridizations are strongly affected by the non-uniform chemical environment. The presence of mixed four-orbital hybridizations implies that it would be difficult to simulate the VASP band structures by employing a tight-binding model with orbital-induced hopping integrals and site energies,[8] and the spin-dependent interactions.[56] The above-mentioned results clearly indicate that there are important differences between the three kinds of guest-atom substitutions. The unusual features of the charge density distributions might be closely related to the strong affinity of the nitrogen atoms.

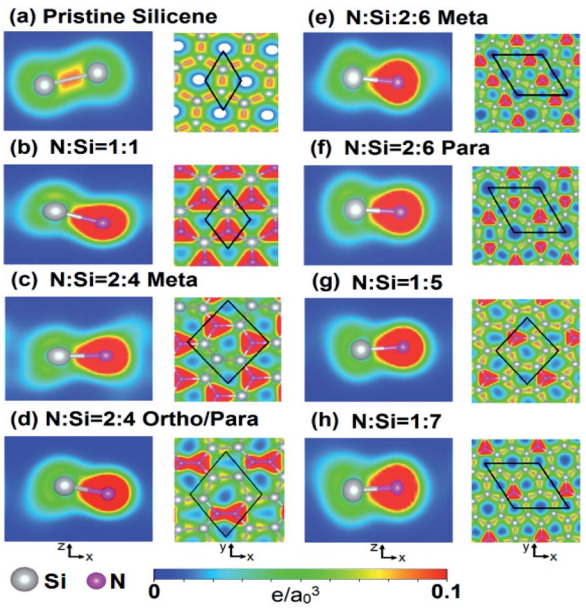

Fig. 3 The spatial charge distributions of nitrogen-substituted silicene materials for various concentrations and configurations: (a) without guest atoms, (b) [1 : 1], (c) [2 : 4]-*meta*, (d) [2 : 4]-*ortho*/*para*, (e) [2 : 6]-*meta*, (f) [2 : 6]-*para*, (g) [1 : 5]-single, and (h) [1 : 7] conditions. The two projections along the [*x*, *z*] and [*x*, *y*] planes clearly indicate the multi-orbital chemical bonding.

The ferromagnetic configurations which occur for certain high-concentration substitutions are clearly revealed in the spatial spin density distributions, as illustrated in Fig. 4(a)–(d) with top and side views. The net magnetic moment is very sensitive to nitrogen concentration [Table 1]. Generally speaking, the spatial spin density distributions are highly non-uniform and anisotropic. For the [1 : 1] case, only the spin-up density could survive in the stable honeycomb lattice of a uniform 2D nitrogen–silicon compound [the red regions in Fig. 4(a)]. Very interestingly, the spin-up density is only revealed in the upper half-plane of $z > 0$ for the host atoms [the gray atoms], while its distribution is nearly symmetric about the center of the guest atoms [the blue atoms]. The highly asymmetric spin distribution could play an important role in the creation of ferromagnetism.[57] The nitrogen-induced red regions are comparable with those associated with the silicon atoms; that is, both make important contributions to the magnetic properties. This result is consistent with the N and Si dominance in the first spin-split valence band below the Fermi level [Fig. 2(b)], and the comparable spin-up densities of states due to the $2p_z$ and $3p_z$ orbitals [discussed later in Fig. 5(b)]. Similar magnetic phenomena are revealed in the [2 : 4]-*meta* case [Fig. 4(b)]. However, some small spin-up density is present in the lower half-plane of $z < 0$, and the weight related to the nitrogen atoms declines quickly. With further decreasing nitrogen concentration, the spin-up and spin-down states start to exist simultaneously [the red and yellow regions], residing on neighboring silicon atoms, *e.g.*, the [1 : 5] and [1 : 7] cases in Fig. 4(c) and (d), respectively. Also, note that the guest N atoms possess some weak spin-up density. Most importantly, the competition between opposite spin configurations leads to a weakened magnetic moment and thus greatly reduces the ferromagnetism.

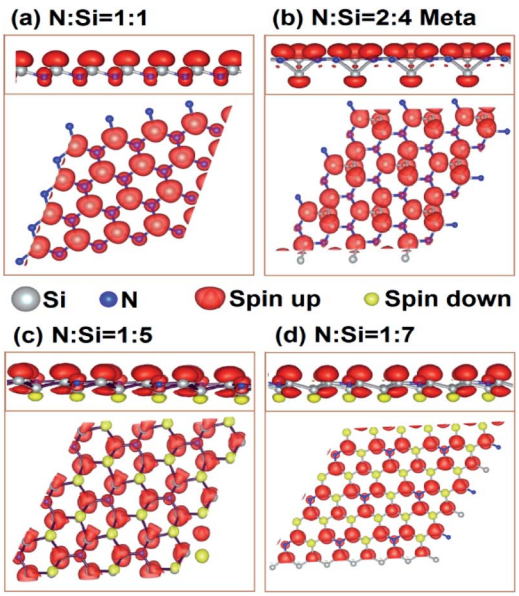

Fig. 4 The spin-charge distributions in nitrogen-substituted silicene systems for certain cases: (a) [1 : 1], (b) [2 : 4]-*meta*, (c) [1 : 5] and (d) [1 : 7], showing top and side views. Red and yellow correspond to spin-up and spin-down, respectively.

The theoretical predictions of the spatial ferromagnetic configurations and the spin-created magnetic moments could be verified by high-resolution SP-STM and SQUID measurements, respectively. Specifically, the non-magnetic configurations mostly occur in the low-concentration cases [<~13% for the ratio of guest to host atoms in Table 1]. Furthermore, the spin-degenerate energy sub-bands correspond to the modified Dirac cone structures [Fig. 2(h)–(j) and (l)]. It seems that the atom-created spin configurations are effectively suppressed by the well-behaved π bonding [the $3p_z$–$3p_z$, $3p_z$–$2p_z$, and $2p_z$–$2p_z$ orbital hybridizations, especially the first ones], *i.e.*, the spin-induced on-site Coulomb potentials[58] have a negligible effect in reducing the total ground state energy, compared with the charge-dependent atomic interactions.[59]

3.4 Density of states

The atom-, orbital- and spin-decomposed density of states are able to provide more information about the complicated orbital hybridizations and spin configurations in nitrogen-substituted silicenes, as clearly illustrated in Fig. 5(a)–(l) for the various substitution cases. There are many special structures in the density of states, mainly owing to the band-edge states of parabolic and oscillatory energy dispersions [Fig. 2(a)–(l)]. These special critical points are closely related to the extremal states in the parabolic sub-bands/modified Dirac cone structures, the partial flat bands along with any direction/a specific direction [the quasi-zero-/one-dimensional parabolic bands], and the saddle-point structures near the high-symmetry point. They create van Hove singularities in the form of shoulders/asymmetric V-shapes, delta-function-like peaks/divergent peaks in the square-root form, and logarithmic peak, respectively. Very interestingly, the modified V-shape structures, which are centered in the range of -0.5 eV $< E < 0$, appear at sufficiently low concentrations, such as the [2 : 16]-*meta*, [2 : 16]-*ortho*, [2 : 16]-*para* and [1 : 17]-single cases [Fig. 5(h)–(j) and (l)]. These results indicate gradual recovery of the Dirac cone structure with decreasing N concentration. According to the density of states near the Fermi level, one can distinguish between semiconducting and metallic behavior. Only the [1 : 1] and [2 : 16]-*meta* cases are clearly semiconductors [Fig. 5(b) and (h)], while the other ones are gapless conductors/semiconductors. Specifically, certain nitrogen-substituted silicenes have sufficiently high numbers of free carriers due to the crossings of partially flat sub-bands with the Fermi level, as clearly illustrated by the large density of states at E_F for the [2 : 6]-*meta*, [2 : 6]-*ortho*, [2 : 6]-*para* and [1 : 7]-single configurations [Fig. 5(e)–(g) and (l)].

The atom-, orbital- and spin-dependent interactions play critical roles in the creation of various van Hove singularities. Roughly speaking, within the energy range of -1.0 eV $< E <$ 1.0 eV, the density of states is dominated by the Si-$3p_z$ and N-$2p_z$ orbitals [the solid and dashed purple curves], with the 3s, $3p_x$, $3p_y$, 2s, $2p_x$, and $2p_y$ orbitals also making significant contributions. Furthermore, the series of extended van Hove singularities, being associated with the π-electronic orbitals,

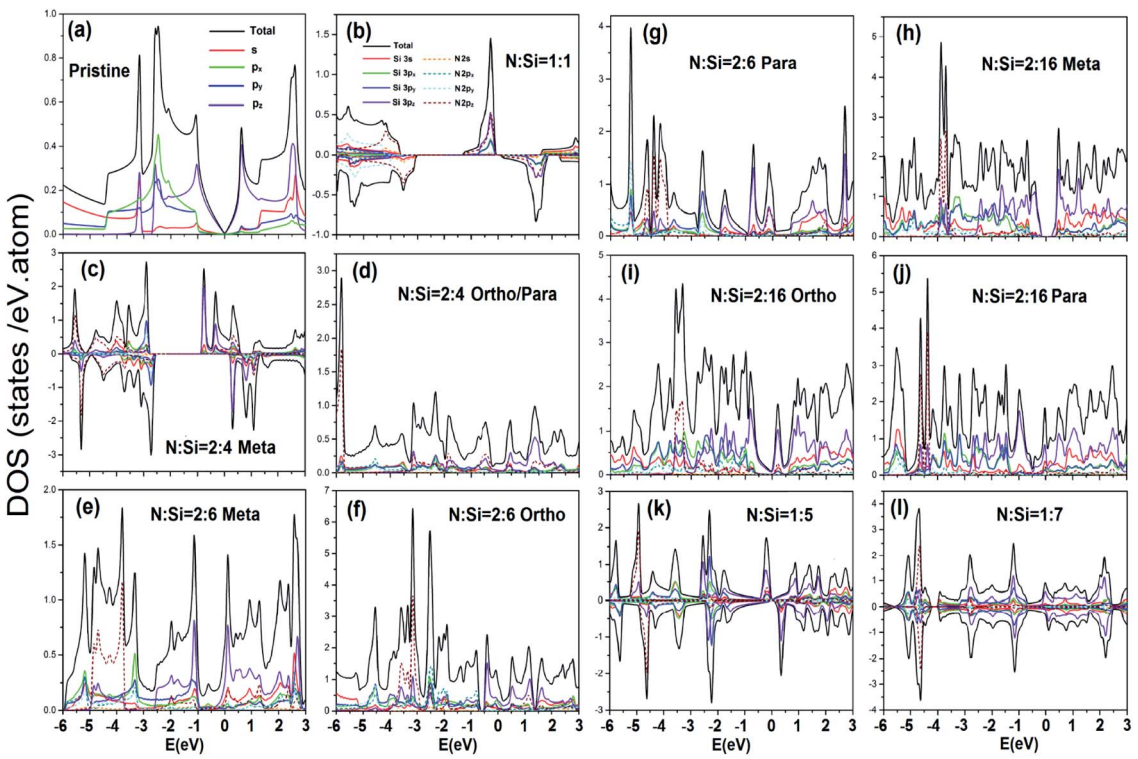

Fig. 5 The atom- and orbital-decomposed density of states of nitrogen-substituted silicenes for various cases: (a) pristine, (b) [1 : 1], (c) [2 : 4]-*meta*, (d) [2 : 4]-*ortho*/*para*, (e) [2 : 6]-*meta*, (f) [2 : 6]-*ortho*, (g) [2 : 6]-*para*, (h) [2 : 16]-*meta*, (i) [2 : 16]-*ortho*, (j) [2 : 16]-*para*, (k) [1 : 5], and (l) [1 : 7]. For ferromagnetic systems, negative DOS corresponds to the spin-down component.

are very difficult to identify among the special structures. As a result, the π and σ sub-bands do not survive in any nitrogen-substituted silicene system. It should be noted that the van Hove singularities due to the eight orbitals of the guest and host atoms might overlap at certain energies. This further illustrates the mixed four-orbital hybridizations in any chemical bond, as observed earlier in the spatial charge distributions [Fig. 3]. Concerning the spin-split density of states, the ferromagnetic configuration is mainly determined by the sub-bands near the Fermi level. The spin-up and spin-down states appear at $E < 0$ and $E > 0$, respectively, such as those of the [1 : 1], [2 : 4]-*meta*, [1 : 5]-single and [1 : 7]-single conditions [Fig. 5(b), (c), (k) and (l)]. Apparently, in the former case, the occupied electronic states account for the net magnetic moment. On the other hand, at lower/higher energies, two kinds of spin arrangements coexist and lead to the absence of ferromagnetism.

High-resolution STS/SP-STS measurements are the most efficient and accurate way of exploring the van Hove singularities of layered materials. They are very suitable for identifying the abundant special structures in the density of states due to the various numbers of layers and stacking configurations of few-layer graphene systems, such as monolayer graphene,[60] AB bilayer and trilayer stackings,[61] twisted bilayer graphenes,[62] and ABC- and AAB-stacked trilayer graphene systems.[63,64] Very interestingly, direct combinations of SP-STM and SP-STS are capable of thoroughly examining the spin-induced magnetic properties. To date, the former is successful in observing magnetic domains and domain-wall structures with a high spatial resolution of 10 nm;[65] furthermore, the latter can distinguish between metallic and semiconducting ferromagnetism.[66] They can be used to verify the unusual special features of nitrogen-substituted silicenes, which include the finite or vanishing density of states at the Fermi level, the special structures due to complicated multi-orbital hybridizations, the modified V-shape near E_F at sufficiently low substitution concentrations, the absence of well-defined π- and σ-band widths, and the low-lying spin-degenerate or spin-split energy spectra. Such examinations could provide further information on the multi-orbital- and spin-dependent interactions.

4 Concluding remarks

Nitrogen-substituted silicene materials exhibit many unusual properties. These include the bond lengths, the total ground state energies, the net/vanishing magnetic moments, the band crossing Fermi level [the semiconducting, semi-metallic and p-type phenomena], the modified Dirac cone structures/the low-lying oscillatory dispersions, the well-defined π and π* sub-bands/the ill-defined π- and σ-states [the π- and σ-orbital bonding/the four-orbital hybridizations], the abundant and complicated σ valence sub-bands, the spin-degenerate/spin-split bands, the frequent crossings/few anticrossings along the ΓM and KM paths, the atom-, orbital- and spin-dependent van Hove singularities, and the highly non-homogeneous spin density distribution for certain N substitution cases.

The N–Si bond lengths could be estimated from the N–N and Si–Si ones, indicating the characteristics of covalent bonds in the silicon-based few-layer compounds. Roughly speaking, the Fermi level is situated in the middle of the modified Dirac cone structures. In general, the initial σ valence sub-bands could be roughly defined from the zone-folding effects. On the other hand, the low-lying non-monotonic sub-bands clearly illustrate the complicated [2s, $2p_x$, $2p_y$, $2p_z$]–/[3s, $3p_x$, $3p_y$, $3p_z$]–[3s, $3p_x$, $3p_y$, $3p_z$] orbital hybridizations in the N–Si/Si–Si bonds. It is almost impossible to clearly characterize the π and σ chemical bonding. The spin-split sub-bands, as well as the net moments and the spatial ferromagnetic configurations could survive only in specific cases, in which the spin states are associated with the guest and host atoms simultaneously. There exist ferromagnetic semiconductors or semi-metals. Furthermore, it is almost impossible to define the blue/red shift of the Fermi level in the absence of a modified Dirac cone structure. Also note that these materials cannot be regarded as n-type materials even with an extra valence electron provided by each nitrogen atom.

Most importantly, substitution-enriched electronic structures are expected to present diverse essential properties. First-principles calculations show that the low-energy electronic states could be approximated by modified Dirac cones [the π chemical bonding] for the carbon- and boron-substituted silicene systems, but not for the nitrogen-containing ones. As to the former, a generalized tight-binding model is available for thorough investigations of the unique magnetic quantizations,[67] the rich magneto-optical absorption spectra, the unusual quantum Hall conductivities,[68] and the various magneto-plasmon modes.[69] Very interestingly, the modulation of the free hole densities by variation of the boron concentration is capable of creating diverse essential properties,[70] but for nitrogen substitutions, the multi-orbital hopping integrals might be too complicated to calculate and the tight-binding model cannot fit the VASP band structures well along the high-symmetry points.[71] Consequently, it would be very difficult to fully explore the above-mentioned magnetic quantization phenomena. However, besides the substitution of guest atoms in silicene, there are other events and phenomena that may occur during experimental growth, such as vacancy defects, heterojunctions, interstitial sites, and vacancy–interstitial pairs, which can be investigated in a similar manner.

Conflicts of interest

There are no conflicts to declare.

Acknowledgements

This work was financially supported by the Hierarchical Green-Energy Materials (Hi-GEM) Research Center, from The Featured Areas Research Center Program within the framework of the Higher Education Sprout Project of the Ministry of Education (MOE) and the Ministry of Science and Technology (MOST 108-3017-F-006-003) in Taiwan.

References

1 K. S. Novoselov, A. K. Geim, S. V. Morozov and D. Jiang, *Nature*, 2005, **438**, 197.
2 R. Arafune, R. Arafune, C. L. Lin, K. Kawahara and N. Tsukahara, *Surf. Sci.*, 2013, **608**, 297–300.
3 L. Meng, Y. Wang, L. Zhang, S. Du, R. Wu and L. Li, *Nano Lett.*, 2013, **13**, 685–690.
4 A. Fleurence, R. Friedlein, T. Ozaki, H. Kawai and Y. Wang, *Phys. Rev. Lett.*, 2012, **108**, 245501.
5 L. Li, S. Lu, J. Pan, Z. Qin and Y. Wang, *Adv. Mater.*, 2014, **26**, 4820–4824.
6 M. E. DÃąvila, L. Xian, S. Cahangirov and A. Rubio, *New J. Phys.*, 2014, **16**, 095002.
7 M. Derivaz, D. Dentel, R. Stephan, M. C. Hanf, A. Mehdaoui, P. Sonnet and C. Pirri, *Nano Lett.*, 2015, **15**, 2510–2516.
8 P. H. Shih, T. N. Do, G. Gumbs, H. D. Pham and M. F. Lin, *Opt. Lett.*, 2019, **44**, 4721–4724.
9 N. T. T. Tran, D. K. Nguyen, S. Y. Lin, G. Gumbs and M. F. Lin, *ChemPhysChem*, 2019, **2019**, 2473–2481.
10 Y. H. Ho, J. Y. Wu, R. B. Chen, Y. H. Chiu and M. F. Lin, *Appl. Phys. Lett.*, 2010, **97**(10), 101905.
11 S. H. Lee, Y. H. Ho, C. W. Chiu and M. F. Lin, *J. Appl. Phys.*, 2010, **108**(4), 043509.
12 G. G. Guzmán-Verri and L. C. L. Y. Voon, *J. Phys.: Condens. Matter*, 2011, **23**(14), 145502.
13 D. K. Nguyen, N. T. T. Tran, Y. H. Chiu and M. F. Lin, *Sci. Rep.*, 2019, **9**(1), 1–15.
14 S. Y. Lin, S. L. Chang, N. T. T. Tran, P. H. Yang and M. F. Lin, *Phys. Chem. Chem. Phys.*, 2015, **17**, 26443.
15 H. C. Huang, S. Y. Lin, C. L. Wu and M. F. Lin, *Carbon*, 2016, **103**, 84–93.
16 H. Wang, Q. Wang, Y. Cheng, K. Li, Y. Yao and Q. Zhang, *Nano Lett.*, 2012, **12**(1), 141–144.
17 B. Huang, F. Liu, J. Wu, B. L. Gu and W. Duan, *Phys. Rev. B: Condens. Matter Mater. Phys.*, 2008, **77**, 153411.
18 B. Feng, H. Li, S. Meng, L. Chen and K. Wu, *Surf. Sci.*, 2016, **645**, 74–79.
19 Y. Li, H. B. Zhu, G. Q. Wang, Y. Z. Peng, J. R. Xu and Z. H. Qian, *Phys. Rev. B*, 2018, **97**, 085427.
20 L. Tao, E. Cinquanta, D. Chiappe and C. Grazianetti, *Nat. Nanotechnol.*, 2015, **10**, 227–231.
21 P. H. Shih, T. N. Do, G. Gumbs, D. Huang, T. P. Pham and M. F. Lin, *Carbon*, 2020, **160**, 211–218.
22 H. Xie, T. Ouyang, E. Germaneau, G. Qin, M. Hu and H. Bao, *Phys. Rev. B*, 2016, **93**, 075404.
23 H. Sahin and F. M. Peeters, *Phys. Rev. B: Condens. Matter Mater. Phys.*, 2013, **87**, 085423.
24 F. Zheng, C. Zhang, P. Wang and S. Li, *J. Appl. Phys.*, 2013, **113**, 154302.
25 N. T. T. Tran, D. Dahal, G. Gumbs and M. F. Lin, *Struct. Chem.*, 2017, **28**, 1311–1318.
26 K. Kakaei and A. Balavandi, *J. Colloid Interface Sci.*, 2016, **463**, 46–54.
27 Y. Li, H. Chen, L. Y. Voo, J. Ji, G. Zhang and G. Zhang, *J. Mater. Chem.*, 2012, **22**, 15021–15024.
28 I. Y. Jeon, H. J. Choi, M. Choi, J. M. Seo, S. M. Jung and M. J. Kim, *Sci. Rep.*, 2013, **3**, 1810.
29 R. Krishna, E. Titus, L. C. Costa and J. C. Menezes, *J. Mater. Chem.*, 2012, **22**, 10457–10459.
30 B. Vertruyen, D. Flahaut, S. Hebert and A. Maignan, *J. Magn. Magn. Mater.*, 2004, **280**(1), 75–83.
31 J. Sivek, H. Sahin, B. Partoens and F. M. Peeters, *Phys. Rev. B: Condens. Matter Mater. Phys.*, 2013, **87**, 085444.
32 M. M. Monshi, S. M. Aghaei and I. Calizo, *Surf. Sci.*, 2017, **665**, 96–102.
33 S. Granjeaud, K. Yckache, M. Dayez, A. Humbert, C. Chapon and C. R. Henry, *Microsc., Microanal., Microstruct.*, 1993, **4**, 409–418.
34 A. Damascelli, *Phys. Scr.*, 2004, **109**, 61–74.
35 D. D. D. Ma, C. S. Lee and S. T. Lee, *Appl. Phys. Lett.*, 2001, **79**, 2468.
36 J. P. Cleuziou, W. Wernsdorfer, V. Bouchiat, T. Ondarcuhu and M. Monthioux, *Nat. Nanotechnol.*, 2006, **1**, 53–59.
37 G. Kresse and J. Furthmüller, *Phys. Rev. B: Condens. Matter Mater. Phys.*, 1996, **54**, 11169.
38 G. Kresse and D. Joubert, *Phys. Rev. B: Condens. Matter Mater. Phys.*, 1999, **59**, 1758.
39 J. P. Perdew, K. Burke and M. Ernzerhof, *Phys. Rev. Lett.*, 1996, **77**, 3865.
40 P. E. Blöchl, *Phys. Rev. B: Condens. Matter Mater. Phys.*, 1994, **50**, 17953.
41 S. C. Chen, J. Y. Wu and M. F. Lin, *New J. Phys.*, 2018, **20**, 062001.
42 S. J. Barraza and S. E. Denmark, *J. Am. Chem. Soc.*, 2018, **140**, 6668–6684.
43 Y. H. Chiu, J. H. Ho, C. P. Chang, D. S. Chuu and M. F. Lin, *Phys. Rev. B*, 2008, **78**, 245411.
44 A. L. Rakhmanov, A. V. Rozhkov and A. O. Sboychakov, *Phys. Rev. Lett.*, 2012, **109**, 206801.
45 P. H. Shih, T. N. Do, G. Gumbs, D. Huang, H. D. Pham and M. F. Lin, *Sci. Rep.*, 2019, **9**, 14799.
46 V. Paul-Boncour, M. Gupta and J. M. Joubert, *J. Mater. Chem.*, 2000, **10**, 2741–2747.
47 A. Ruegg and G. A. Fiete, *Phys. Rev. B: Condens. Matter Mater. Phys.*, 2011, **84**, 201103.
48 J. Sivek, H. Sahin, B. Partoens and F. M. Peeters, *Phys. Rev. B: Condens. Matter Mater. Phys.*, 2013, **87**, 085444.
49 B. Partoens and F. M. Peeters, *Phys. Rev. B: Condens. Matter Mater. Phys.*, 2006, **74**, 075404.
50 P. H. Shih, T. N. Do, B. L. Huang, G. Gumbs, D. Huang and M. F. Lin, *Carbon*, 2019, **144**, 608–614.
51 S. L. Chang, S. Y. Lin, S. K. Lin, C. H. Lee and M. F. Lin, *Sci. Rep.*, 2014, **4**, 6038.
52 S. Y. Lin, S. L. Chang, H. H. Chen, S. H. Su and M. F. Lin, *Phys. Chem. Chem. Phys.*, 2016, **18**, 18978.
53 S. V. Eremeev, G. Landolt and T. V. Menshchikova, *Nat. Commun.*, 2012, **3**, 635.
54 N. T. T. Tran, D. K. Nguyen, O. E. Glukhova and M. F. Lin, *Sci. Rep.*, 2017, **7**, 17858.
55 L. Chen, B. Feng and K. Wu, *Appl. Phys. Lett.*, 2013, **102**, 081602.

56 J. Y. Wu, S. C. Chen, G. Gumbs and M. F. Lin, *Phys. Rev. B*, 2016, **94**, 205427.
57 J. Y. Wu, C. Y. Lin, G. Gumbs and M. F. Lin, *RSC Adv.*, 2015, **5**, 51912.
58 S. C. Chen, C. L. Wu, J. Y. Wu and M. F. Lin, *Phys. Rev. B*, 2016, **94**, 045410.
59 T. J. Giese and D. M. York, *J. Chem. Phys.*, 2005, **123**, 164108.
60 H. H. Chen, S. H. Su, S. L. Chang, B. Y. Cheng, C. W. Chong and M. F. Lin, *Carbon*, 2015, **93**, 180–186.
61 Y. C. Chuang, J. Y. Wu and M. F. Lin, *Sci. Rep.*, 2013, **3**, 1368.
62 J. F. Dodaro, S. A. Kivelson, Y. Schattner, X. Q. Sun and C. Wang, *Phys. Rev. B*, 2018, **98**, 075154.
63 C. Y. Lin, M. H. Lee and M. F. Lin, *Phys. Rev. B*, 2018, **98**, 041408.
64 C. Y. Lin, B. L. Huang, C. H. Ho, G. Gumbs and M. F. Lin, *Phys. Rev. B*, 2018, **98**, 195442.
65 C. Chen, N. Hayazawa and S. Kawata, *Nat. Commun.*, 2014, **5**, 3312.
66 I. Felner, U. Asaf, Y. Levi and O. Millo, *Phys. C*, 2000, **334**, 141–151.
67 J. Y. Wu, S. C. Chen, G. Gumbs and M. F. Lin, *Phys. Rev. B*, 2017, **95**, 115411.
68 T. N. Do, G. Gumbs, P. H. Shih, D. Huang and M. F. Lin, *Phys. Rev. B*, 2019, **100**, 155403.
69 G. Gumbs, A. Iurov, J. Y. Wu, M. F. Lin and P. Fekete, *Phys. Rev. B*, 2016, **100**, 155403.
70 J. C. Axtell, L. M. A. Saleh, E. A. Qian and A. I. Wixtrom, *Inorg. Chem.*, 2018, **57**, 2333–2350.
71 C. C. Liu, W. Feng and Y. Yao, *Phys. Rev. Lett.*, 2011, **107**, 076802.